Computation of the Semiclassical Limit of the Schrödinger Equation with Phase Shift by a Level Set Method

Shi Jin and Xu Yang *

Abstract

In this paper, we show how the level set method, developed in [18, 7, 17] for the numerical computation of the semiclassical limit of the Schrödinger equation, can be amended to include the phase shift using the Keller-Maslov index. This gives a more accurate approximation of the physical observables for multivalued solutions in the semiclassical limit. Numerical examples in one and two spaces dimensions demonstrate the improved accuracy of our approach away from caustics.

1 Introduction

We are interested in an efficient numerical method to solve the linear Schrödinger equation with the high frequency initial data:

$$i\epsilon\frac{\partial\Psi^\epsilon}{\partial t}+\frac{\epsilon^2}{2}\Delta\Psi^\epsilon-V(\mathbf{x})\Psi^\epsilon=0,\quad \mathbf{x}\in\mathbb{R}^n\,, \tag{1.1}$$

$$\Psi^\epsilon(\mathbf{x},0)=A_0(\mathbf{x})e^{iS_0(\mathbf{x})/\epsilon}\,. \tag{1.2}$$

In (1.1), $\Psi^\epsilon(\mathbf{x},t)$ is the wave function, ϵ is the re-scaled Plank constant, and $V(\mathbf{x})$ is the smooth potential. One can define the so-called physical observables from the wave function:

$$\text{position density}\quad n^\epsilon = |\Psi^\epsilon|^2\,, \tag{1.3}$$

$$\text{density flux}\quad J^\epsilon = \frac{\epsilon}{2i}\left(\Psi^\epsilon\nabla\overline{\Psi^\epsilon}-\overline{\Psi^\epsilon}\nabla\Psi^\epsilon\right), \tag{1.4}$$

$$\text{kinetic energy}\quad E^\epsilon = \frac{\epsilon^2}{2}|\nabla\Psi^\epsilon|^2\,. \tag{1.5}$$

In the semiclassical regime, where ϵ is small, the wave function $\Psi^\epsilon(\mathbf{x},t)$ and the related physical observables become oscillatory of wave length $O(\epsilon)$. Typically, a direct simulation

*Department of Mathematics, University of Wisconsin, Madison, WI 53706. Emails: jin@math.wisc.edu, xyang@math.wisc.edu. Research supported by NSF grant No. DMS-0608720.

to (1.1)-(1.2) require mesh sizes and time steps to be $o(\epsilon)$ if a finite difference method is used [21, 22], or a mesh size of $O(\epsilon)$ when using the time-splitting spectral method [1]. The mesh strategy makes the computation of the solution to (1.1)-(1.2) extremely expensive, especially in high dimensions.

A more efficient approach is to solve the asymptotic equation by letting ϵ go to zero. The classical WKB analysis applies the ansatz

$$\Psi^\epsilon(\mathbf{x},t) = A(\mathbf{x},t)e^{iS(\mathbf{x},t)/\epsilon}$$

to (1.1)-(1.2), which gives, to the leading order, the eikonal equation for the phase $S(\mathbf{x},t)$ and the transport equation for the amplitude $\rho(\mathbf{x},t) = |A(\mathbf{x},t)|^2$([28]):

$$S_t + \frac{1}{2}|\nabla S|^2 + V(\mathbf{x}) = 0\,, \tag{1.6}$$

$$\rho_t + \nabla\cdot(\rho\nabla S) = 0\,. \tag{1.7}$$

Since the eikonal equation (1.6) is the Hamilton-Jacobi type, it could become singular (caustic formation) even if the initial profile is smooth. Beyond the singularity a standard numerical scheme using the shock capturing ideas will select the viscous solution [9] [20], which is not the correct semiclassical limit of the Schrödinger equation (1.1) since the linear superposition principle is violated. The semiclassical limit solution becomes *multivalued* after the caustic formation, which can be studied-in the constant potential case– by the stationary phase method [11, 4], or the Fourier Integral Operators [8, 23] for variable potentials. Here we summarize the result of [23] for the Schrödinger equation in Theorem 1.2.

Definition 1.1. The ray trajectory $\mathbf{q}(s,\mathbf{y})$ is given by the Hamilton system corresponding to the eiconal equation (1.6), i.e.

$$\frac{d\mathbf{q}(s,\mathbf{y})}{ds} = \mathbf{p}(s,\mathbf{y}), \quad \frac{d\mathbf{p}(s,\mathbf{y})}{ds} = -V_{\mathbf{q}}(\mathbf{q}),$$

with the initial condition

$$\mathbf{q}(0,\mathbf{y}) = \mathbf{y}, \quad \mathbf{p}(0,\mathbf{y}) = \frac{\partial S_0(\mathbf{y})}{\partial \mathbf{y}}.$$

Theorem 1.2. *As $\epsilon\to 0$, away from the caustic points,*

$$\Psi^\epsilon(\boldsymbol{x},t) \;=\; \sum_{k=1}^{K} \frac{A_0(\boldsymbol{y}_k)}{\sqrt{\left|\det\frac{\partial \boldsymbol{q}(t,\boldsymbol{y}_k)}{\partial \boldsymbol{y}}\right|}} \exp\left(\frac{i}{\epsilon}S_k(\boldsymbol{x},t) + \frac{i\pi}{4}\mu_k\right) + O(\epsilon) \tag{1.8}$$

where $\boldsymbol{y}_k$, $k=1,\cdots,K<\infty$, are all points such that there exists one classical ray trajectory $\boldsymbol{q}(s,\boldsymbol{y}_k)$ joining the points $\boldsymbol{y}_k$ and $\boldsymbol{x}$, i.e. $\boldsymbol{q}|_{s=0} = \boldsymbol{y}_k$, $\boldsymbol{q}|_{s=t} = \boldsymbol{x}$. The phase is given by

$$S_k(\boldsymbol{x},t) = S_0(\boldsymbol{y}_k) + \int_0^t \left(\frac{\dot{\boldsymbol{q}}^2}{2} - V(\boldsymbol{q})\right) ds,$$

in which the line integral is taken along the ray trajectory $\boldsymbol{q}(s, \boldsymbol{y}_k)$ *and* $\dot{\boldsymbol{q}} = \dfrac{d\boldsymbol{q}(s, \boldsymbol{y}_k)}{ds}$. $\mu_k = -2m_k$ *is the Keller-Maslov index of the ray* $\boldsymbol{q}(s, \boldsymbol{y}_k)$*, where* m_k *(the Morse index) is the number of zeros of the Jacobian* $J(t, \boldsymbol{y}_k) = \det \dfrac{\partial \boldsymbol{q}(t, \boldsymbol{y}_k)}{\partial \boldsymbol{y}}$ *on the ray (including their multiplicities).* m_k *also equals to the number of the contact points of ray* $\boldsymbol{q}(s, \boldsymbol{y}_k)$ *with the caustic of ray family* $\{\boldsymbol{q} = \boldsymbol{q}(t, \boldsymbol{y})\}$ *within time* $0 \le s \le t$.

Remark 1.3. If $V(x)$ is constant, we have the following explicit formula by the stationary phase method,

$$\Psi^\epsilon(\mathbf{x}, t) \;=\; \sum_{k=1}^{K} \frac{A_0(\mathbf{y}_k)}{\sqrt{|1 + tD^2 S_0(\mathbf{y}_k)|}} \exp\left(\frac{i}{\epsilon} S(\xi_k, \mathbf{y}_k) + \frac{i\pi}{4}\mu_k\right) + O(\epsilon) \tag{1.9}$$

where the phase

$$S(\xi, \mathbf{y}) = \xi \cdot \mathbf{x} - \xi \cdot \mathbf{y} - (1/2)\,|\xi|^2\, t + S_0(y),$$

has finitely many ($K < \infty$) stationary phases ξ_k and $\mathbf{y}_k$:

$$\xi_k = \nabla S_0(\mathbf{y}_k), \quad \mathbf{y}_k = \mathbf{x} - t\nabla S_0(\mathbf{y}_k)\,,$$

D^2 stands for the Hessian matrix, while $\mu_k = \mathrm{sgn}(D^2 S(\xi_k, \mathbf{y}_k))$ is the Keller-Maslov index of the kth ray.

Denoting

$$A_k(\mathbf{x}, t) = \frac{A_0(\mathbf{y}_k)}{\sqrt{\left|\det \frac{\partial \mathbf{q}(t, \mathbf{y}_k)}{\partial \mathbf{y}}\right|}},$$

then Theorem 1.1 shows that

$$\Psi^\epsilon = \sum_{k=1}^{K} A_k(\mathbf{x}, t) \exp(\tfrac{i\pi}{4}\mu_k) \exp(\tfrac{i}{\epsilon} S_k(\mathbf{x}, t)) + O(\epsilon)\,. \tag{1.10}$$

Thus, as $\epsilon \to 0$, $\Psi^\epsilon(\mathbf{x}, t)$ is a linear superposition of K-branches, each of which (A_k, S_k) solves the eiconal and transport equations (1.6)-(1.7), with a phase shift determined by $-\mu_k \pi/4$ at caustics.

In the last few years, the level set method has been proposed to to compute the multivalued solutions of the semiclassical limit of the Schrödinger equation [18, 7, 17]. The idea of the level set method is to build the solution of the phase S (or more specifically, the velocity $u = \nabla S$) into the intersection of zero level sets of phase-space functions, which can be shown to satisfy the linear Liouville equations, the intersection of whose zero level sets gives the multivalued velocity or phases. The physical observables can be obtained via the evaluations of singular integrals involving the level set functions. Although these Liouville equations are defined in the phase space, by using the local level set method [25, 26, 27], the computational cost is almost linear in the number of grid points in the physical domain. Compared

with the moment methods [5, 10, 14, 16], the level set method is simple and more robust in the case of large K and high space dimension. When compared with the approach using the semiclassical limit based on the Wigner transform [19, 13, 29], the level set method has the advantage of avoiding the numerical evolution of measure-valued solutions, thus gives a much better numerical resolution [17].

However, none of the aforementioned approaches (the level set method, the moment method, or the method based on the Wigner transform) correctly captures the phase shift. (We mention the work of Benamou [2, 3] that uses the so-called big tracing tracing for multivalued solutions with phase shift for the fold caustic cases). This will result in phase errors when the physical observables are computed. The aim of this paper is to incorporate the phase shift into the level set method of [18, 7, 17] so more accurate physical observables can be obtained numerically. The basis of our approach is Theorem 1.1.

The paper is organized as follows: in Section 2, we summarize the formal level set method for the computation of the multivalued velocities and densities ([18, 17]); in Section 3, we show how the level set method can be amended to include the correct phase shift. The method in higher space dimensions is described in Section 4. In Section 5, numerical examples in both 1d and 2d are given to show the imporved accuracy, when compared with previous methods, of the current approach.

2 The Level Set Method for Multivalued Solution

We first review the level set method developed in [18, 7, 17] for the numerical computation of multivalued velocity and density that arise in the semiclassical limit of the linear Schrödinger equation.

2.1 Multivalued velocity

Consider the time dependent, n-dimensional Hamilton-Jacobi equation

$$\partial_t S + H(\mathbf{x}, \nabla S) = 0, \tag{2.1}$$

$$S(0, \mathbf{x}) = S_0(\mathbf{x}). \tag{2.2}$$

Note that the eikonal equation (1.6) is a Hamilton-Jacobi equation (2.1) with $H(x, \nabla S) = \frac{1}{2}|\nabla S|^2 + V(\mathbf{x})$.

Introduce $\mathbf{u} = (u_1, \cdots, u_n) = \nabla S$. Taking the gradient on (2.1), one gets

$$\partial_t \mathbf{u} + \nabla_{\mathbf{x}} H(\mathbf{x}, \mathbf{u}) = 0, \tag{2.3}$$

$$\mathbf{u}(0, \mathbf{x}) \equiv \mathbf{u}_0(\mathbf{x}) = \nabla_{\mathbf{x}} S_0(\mathbf{x}). \tag{2.4}$$

Define n level set functions $\varphi_j = \varphi_i(t, \mathbf{x}, \mathbf{p})$, $j = 1, \cdots, n$, where $\mathbf{p} = (p_1, \cdots, p_n) \in \mathbb{R}^n$, such that the intersection of their zero level sets yields multivalued velocity $\mathbf{u}$, namely,

$$\varphi_j(t, \mathbf{x}, \mathbf{p}) = 0 \quad \text{at } \mathbf{p} = \mathbf{u}(t, \mathbf{x}), \quad j = 1, \cdots, d. \tag{2.5}$$

One can show that each φ_j will solve the following initial value problem of the linear Liouville equation:

$$\begin{cases} \partial_t \varphi_j + \nabla_{\mathbf{p}} H \cdot \nabla_{\mathbf{x}} \varphi_j - \nabla_{\mathbf{x}} H \cdot \nabla_{\mathbf{p}} \varphi_j = 0, \quad j = 1, \cdots, n\,, \\ \varphi_j(0, \mathbf{x}, \mathbf{p}) = p_j - u_j(0, \mathbf{x})\,. \end{cases} \tag{2.6}$$

For discontinuous $u_j(0, x)$, the signed distance function is used such that each ϕ_j is always a continuous function.

2.2 Multivalued density

The multivalued density is given by

$$\rho(\mathbf{x}) = \int_{\mathbb{R}^n} \psi(\mathbf{x}, \mathbf{k}, t) \Pi_{j=1}^d \delta(\varphi_j(\mathbf{x}, \mathbf{k})) d\mathbf{k},$$

where ψ solves the same Liouville equation as (2.6) but with a different initial condition,

$$\begin{cases} \partial_t \psi + \nabla_{\mathbf{p}} H \cdot \nabla_{\mathbf{x}} \psi - \nabla_{\mathbf{x}} H \cdot \nabla_{\mathbf{p}} \psi = 0, \\ \psi_0 = \rho_0(\mathbf{x}) = |A_0(\mathbf{x})|^2\,, \end{cases} \tag{2.7}$$

in which $A_0(x)$ is given in (1.2).

If $\varphi_j(0, x, p)$ is given by the signed distance function, then ψ_0 will be defined differently, after taking the Jacobian of φ_j into consideration. See [17].

3 The Level Set Method with Phase Shift

In this section we show how, in one space dimension, the level set method can be amended to include the phase shift.

- Step 1, solve the multivalued velocities using (2.6).

  Note that for the Schrödinger equation, the Hamiltonian $H(x, p)$ is given by $H(x, p) = \frac{1}{2}|p|^2 + V(x)$. Then one can use a finite volume method to solve the Liouville equation (2.6).

  $$(\varphi_{jl})_t + p_l \frac{\varphi_{j+\frac{1}{2},l} - \varphi_{j-\frac{1}{2},l}}{\Delta x} - \frac{V(x_{j+1}) - V(x_{j-1})}{2\Delta x} \cdot \frac{\varphi_{j,l+\frac{1}{2}} - \varphi_{j,l-\frac{1}{2}}}{\Delta p} = 0\,,$$

  where Δx and Δp are the mesh sizes in the x and p directions respectively, $x_{j+\frac{1}{2}}$ and $p_{l+\frac{1}{2}}$ are the grid points, $x_j = \frac{1}{2}(x_{j-\frac{1}{2}} + x_{j+\frac{1}{2}})$ and $p_l = \frac{1}{2}(p_{l-\frac{1}{2}} + p_{l+\frac{1}{2}})$ are the centers of the cell,

  $$\varphi_{jl} = \frac{1}{\Delta x \Delta p} \int_{x_{j-\frac{1}{2}}}^{x_{j+\frac{1}{2}}} \int_{p_{l-\frac{1}{2}}}^{p_{l+\frac{1}{2}}} \varphi(x, p, t) dp dx$$

  is the cell average, while the fluxes in x and p directions, $\varphi_{j+\frac{1}{2},l}$ and $\varphi_{j,l+\frac{1}{2}}$ are given by some shock capturing method.

- Step 2, at time t, determine the caustic points. In the contour $\varphi(t,x,p(x))=0$, which is a curve in the $x-p$ plane, $p_x(x)=\infty$ at the caustic points which divide the contour curve into several single-valued branches. These branches are the multivalued velocities, denoted by u_k, $k=1,\cdots,K$, where K is the total number of the branches. Define $\varphi^{(k)}(t,x,p(x))=0$ as the part of curve corresponding to the kth branch of the velocity, i.e. $\varphi(t,x,u_k(x))=0$.

  Now we use the level set function φ to rewrite the caustic detection condition:

$$\varphi(t,x,p(x))=0 \Rightarrow \varphi_x(t,x,p(x))+\varphi_p(t,x,p(x))p_x(x)=0\,.$$

  This implies that

$$\varphi_p(t,x,p(x))=0 \tag{3.1}$$

  because $p_x(x)=\infty$ at the caustic points, and φ_x is continuous and bounded.

  Actually, in the cusp caustic case, the caustic points are the single roots of $\varphi_p(t,x,p)=0$ by its definition, so instead we can check the change of sign of $(\varphi_{j,l+\frac{1}{2}}-\varphi_{j,l-\frac{1}{2}})/\Delta p$ for the contour curve points $(x,p(x))$, i.e. $\varphi(t,x,p(x))=0$. If the sign of $(\varphi_{j,l+\frac{1}{2}}-\varphi_{j,l-\frac{1}{2}})/\Delta p$ changes from $(x_j,p(x_j))$ to $(x_{j+1},p(x_{j+1}))$, there must be a caustic in the domain $[x_j,x_{j+1}]\times[p(x_j),p(x_{j+1})]$ because $\varphi_p(t,x,p)=0$ due to the continuity of φ and the Intermediate Value Theorem.

- Step 3, find multivalued ρ_k using multivalued velocities u_k, $k=1,\cdots,K$, by solving (2.7) using the same numerical method as in Step 1.

  The single-valued density branch is given by

$$\rho_k(t,x)=\int \psi(t,x,p)\delta(\varphi^{(k)}(t,x,p))dp=\psi(t,x,u_k(x))\cdot\frac{1}{|\varphi_p(t,x,u_k(x))|}\,. \tag{3.2}$$

  Since the density will blow up if and only if at the caustic points, (3.2) will imply the caustic detection condition is $\varphi_p(t,x,p)=0$ which is exactly (3.1).

  Numerically, to find $\rho_k(t,x_j)$, if $u_k(x_j)$ is not a mesh point in the p-direction, we use the linear interpolation to approximate $\psi(t,x_j,u_k(x_j))$ and $\varphi_p(t,x_j,u_k(x_j))$ by their values at two adjacent points in the p-direction that bound $u_k(x_j)$.

- Step 4, computation of the multivalued phases. One way to do it was to use the level set method as follows (see [7]):

  Define $\tilde{\varphi}(t,x,p,q)=0$ at $p=u$, $q=S$, then one has another linear Liouville equation with the initial condition,

$$\begin{cases} \partial_t\tilde{\varphi}+\partial_p H\partial_x\tilde{\varphi}-\partial_x H\partial_p\tilde{\varphi}+(p\partial_p H-H)\partial_z\tilde{\varphi}=0, \\ \tilde{\varphi}(0,x,p,z)=z-S_0(x), \end{cases} \tag{3.3}$$

where $S_0(x)$ is the initial phase in (1.2). One can get the multivalued phases from the two-dimensional surface $\tilde{\varphi}(t, x, p, q(x, p)) = 0$. Here, in stead of adding more dimensions, we use a generalized (to a variable potential) version of the numerical method proposed by Gosse [14] which allows the computation of the multivalued phase from the multivalued velocity in the physical space. The idea is to do numerical integration (using a quadrature rule) following each branch of the velocity. The integration constants are obtained by both imposing boundary/decay/radiation conditions and the fact that the multivalued phase is continuous which means different branches touch each other when it passes from one branch to the other.

If $u = \partial_x S$, the correct phase is given by [14]

$$S(t, x) = -V(a)t + \int_a^x u(t, s)ds, \quad x \in [a, b]\,. \tag{3.4}$$

Clearly, $S(t, x)$ satisfies the one-dimensional eiconal equation (1.6). One needs to choose the computational domain big enough to have $\partial_x S(t, a) = 0$.

- Step 5, recover the amplitude A_k from ρ_k by the formula

$$A_k(x) = \sqrt{\rho_k}\, \exp\left(i\frac{\pi\mu_k}{4}\right)\,,$$

where μ_k is the Keller-Maslov index.

We finally define the numerical wave function as

$$\Phi(x, t) = \Sigma_k A_k\, \exp\left(i\frac{S_k}{\epsilon}\right). \tag{3.5}$$

Remark 3.1. When one solves the Liouville equations, there is no small scale, so one does not need to resolve ϵ numerically. However, because of the term $\exp(iS/\epsilon)$ in (3.5), the numerical error in S will affect the phase unless ϵ is suitably resolved. For a numerical method of order n, the phase error is in the order of $(\Delta x)^n/\epsilon$. Thus one should use $\Delta x \ll \epsilon^{1/n}$. Clearly, a higher order method is preferred here when solving for the phase S.

4 Generalization to Higher Dimensions

The idea in 1d can be generalized to higher dimensions in a natural way except one needs a rule to detect the caustic curves in higher dimensions. Here we take the 2d problem as an example, and we believe the higher dimensional cases can be dealt with similarly.

- Step 1, solve the multivalued velocities: take $n = 2$ and solve (2.6) numerically for φ_1 and φ_2.

  To visualize the solution which is an intersection of zeros of two level set functions, one may use the technique developed in [24].

- Step 2, the caustic detection and the multivalued densities. Solve (2.7) for ψ, then

$$\rho(t,\mathbf{x}) = \int \psi(t,\mathbf{x},\mathbf{p})\Pi_{j=1}^{2}\delta(\varphi_j(t,\mathbf{x},\mathbf{p}))d\mathbf{p} = \psi(t,\mathbf{x},\mathbf{u}(\mathbf{x}))\cdot\frac{1}{|\det J|} \tag{4.1}$$

where $J = \begin{pmatrix} \frac{\partial\varphi_1}{\partial u_1} & \frac{\partial\varphi_1}{\partial u_2} \\ \frac{\partial\varphi_2}{\partial u_1} & \frac{\partial\varphi_2}{\partial u_2} \end{pmatrix}$ is the Jacobi matrix.

Since the density will blow up if and only if at the caustic points, one obtains the caustic detection condition in 2d as $|\det J| = 0$.

- Step 3, by the caustic detection condition given in Step 2, one can divide the multivalued velocity into several single-valued branches u_k. Similar to 1d,

$$\rho_k(t,\mathbf{x}) = \int \psi(t,\mathbf{x},\mathbf{p})\Pi_{j=1}^{2}\delta(\varphi_j^{(k)}(t,\mathbf{x},\mathbf{p}))d\mathbf{p}$$

will give each branch of density by plugging in the corresponding branch of velocity, where $\varphi_j^{(k)}(t,\mathbf{x},\mathbf{p}) = 0$, $j = 1,2$ is the part of surface corresponding to the kth single-valued branch of the velocity. After that, generalize Gosse's idea [14] to 2d to recover the phase. The only difference lies in that one needs to compute a line integral instead, i.e.

$$S(t,x,y) = -V(a_1,a_2)t + \int_{a_1}^{x} u(t,s,a_2)ds + \int_{a_2}^{y} v(t,x,s)ds, \tag{4.2}$$

where $u = \dfrac{\partial S}{\partial x}$ is the x-component of the velocity, $v = \dfrac{\partial S}{\partial y}$ is the y-component of the velocity, and $(x,y) \in [a_1,b_1]\times[a_2,b_2]$. Then use the ansatz (3.5) to obtain the numerical approximation Φ with the correct phase shift.

(4.2) can be verified in the following way:

$$\int_{a_1}^{x} u(t,s,a_2)ds = \int_{a_1}^{x}\frac{\partial S}{\partial x}(t,s,a_2)ds = S(t,x,a_2) - S(t,a_1,a_2), \tag{4.3}$$

$$\int_{a_2}^{y} v(t,x,s)ds = \int_{a_2}^{y}\frac{\partial S}{\partial y}(t,x,s)ds = S(t,x,y) - S(t,x,a_2). \tag{4.4}$$

Besides, if one takes a large enough domain to make $u(t,a_1,a_2) = 0$, and $v(t,a_1,a_2) = 0$, then by the eiconal equation (1.6),

$$\begin{aligned} & S_t(t,a_1,a_2) = -\frac{1}{2}(u^2(t,a_1,a_2) + v^2(t,a_1,a_2)) - V(a_1,a_2) \\ \Longrightarrow \quad & S_t(t,a_1,a_2) = -V(a_1,a_2) \Rightarrow S(t,a_1,a_2) = -V(a_1,a_2)t + \text{Constant}. \end{aligned} \tag{4.5}$$

Combine (4.3) (4.4) and (4.5), one has (4.2). Note that we drop out the constant in (4.5) because it doesn't affect the quadratic physical observables.

5 The numerical experiments

In this section, we compare the numerical solution of the Schrödinger equation Ψ with the numerical solutions of Φ_1, the semiclassical limit with the phase shift,

$$\Phi_1(x,t) \;=\; \Sigma_j \sqrt{\rho_j}\, \exp\left(i\frac{\pi\mu_j}{4}\right) \exp\left(\frac{S_j}{\epsilon}\right) \tag{5.1}$$

Φ_2, the semiclassical limit without the phase shift,

$$\Phi_2(x,t) \;=\; \Sigma_j \sqrt{\rho_j}\, \exp\left(\frac{S_j}{\epsilon}\right). \tag{5.2}$$

We will only compare the physical observables defined in (1.3)-(1.5) from these wave functions. For the position density, we will also compare the results with Φ_3, the linearly superimposed density, which is what obtained if a moment method for multivalued solution is used [16]:

$$\Phi_3(x,t) \;=\; \sqrt{\Sigma_j \rho_j}\,. \tag{5.3}$$

.

It was already known that the position density $n^\epsilon = |\Psi^\epsilon|^2$ converges to Φ_3^2 weakly as $\epsilon \to 0$, see [12]. With the correct phase shift, our numerical results show a strong L^1 convergence, i.e. $\lim\limits_{\epsilon\to 0} \int ||\Psi^\epsilon| - |\Phi_1||\, dx = 0$.

We use the Strang Splitting Spectral Method (SP2) advocated in [1] to solve the Schrödinger equation with high oscillation initial conditions. Let x_j, $j = 0, \cdots, M-1$ be the mesh points, $t_n = n\Delta t$ $(n = 0, 1, \cdots)$ with Δt the time step, $\Psi_j^{\epsilon,n}$ the numerical approximation of $\Psi^\epsilon(x,t)$ at (x_j, t_n). Then from $t = t_n$ to time $t = t_{n+1}$, the algorithm is summarized as follows:

$$\begin{aligned}
\Psi_j^{\epsilon,*} &= \exp\left(\frac{-iV(x_j)\Delta t}{2\epsilon}\right)\Psi_j^{\epsilon,n},\\
\Psi_j^{\epsilon,**} &= \mathcal{F}^{-1}\left(\mathcal{F}(\Psi_j^{\epsilon,*})\cdot \exp\left(\frac{-i\epsilon\,|k|^2\,\Delta t}{2}\right)\right),\\
\Psi_j^{\epsilon,n+1} &= \exp\left(\frac{-iV(x_j)\Delta t}{2\epsilon}\right)\Psi_j^{\epsilon,**},
\end{aligned}$$

where $\mathcal{F}$ and $\mathcal{F}^{-1}$ are the Fast Fourier Transform and the Fast Inverse Fourier Transform respectively.

The SP2 has been shown to be attractive in giving accurate quadratic observables ([1]). If the wave function is needed then extra care maybe needed to get the accurate phase information (see [6]).

In all one dimensional numerical examples, to solve the Liouville equation, we use the second order Runge-Kutta method for the time discretization and second order upwind

scheme with the minmod slope limiter for the space fluxes. We use a larger domain in both x and p to avoid dealing with the boundary conditions. Periodic conditions are used in the computational domain $[-1,1]\times[-2,2]$. The mesh size is $\Delta x=\Delta p=\dfrac{1}{256}$, and the time step is $\Delta t=\dfrac{1}{1000}$. If one uses the forward Euler scheme in time discretization, the time step will be reduced to $\Delta t=\dfrac{1}{6400}$ or less. The results are shown at time $t=0.5$. And for the Schrödinger equation, the initial conditions are chosen to decay very fast at the boundaries to make sure the periodic boundary conditions do not introduce a significant error relative to the whole space problem in the SP2 method. The mesh size is $\Delta x=\dfrac{1}{16384}$ and the time step is $\Delta t=\dfrac{1}{1000}$. Therefore, to compute Φ_1, the computational cost is $O(256\ln 256)\approx O(1410)$ if the local level set method ([25, 26, 27]) is used. However, to solve the Schrödinger equation, the cost is $O(16384)$. Hence, the computation of Φ_1 will be much more efficient computationally.

Without loss of generality, we can choose $S(t,x)=0$ at $x=-0.5$ as the boundary conditions for recovering the phases from the velocities by (3.4). Whatever the boundary conditions one chooses for $S(t,x)$, it has no effect when we compare the amplitudes, position density fluxes and kinetic energies, since $\left|e^{i\theta}\right|=1,\ \forall\theta\in\mathbb{R}$. The trapezoid method is used to approximate the integrals in (3.4) and (4.2). The phase boundary condition in 2d problem is $S(t,x,y)=0$ at $x=-0.5, y=-0.5$.

In the harmonic oscillator potential example (Example 2), the Morse index given by Theorem 1.2 is

$$m_j=\begin{cases}0, & \text{if } j \text{ is odd};\\ 1 & \text{if } j \text{ is even},\end{cases}$$

which gives

$$\mu_j=\begin{cases}0, & \text{if } j \text{ is odd};\\ -2 & \text{if } j \text{ is even}.\end{cases}\tag{5.4}$$

Note that (5.4) is true for all the cusp caustic cases.

For the other 1d examples where the potential is constant, by Remark 1.3, the Keller-Maslov indexes are

$$\mu_j=\begin{cases}0, & \text{if } j \text{ is odd};\\ -2 & \text{if } j \text{ is even}.\end{cases}\tag{5.5}$$

which is consistent with (5.4) given by Theorem 1.2.

In the two dimensional example, we use the same numerical methods as in the one dimensional examples, with dimensional splitting. the mesh sizes are $\Delta x=\Delta y=\Delta u=\Delta v=\dfrac{1}{256}$ to solve the Liouville equation and $\Delta x=\Delta y=\dfrac{1}{16384}$ to solve the Schrödinger equation. $\Delta t=\dfrac{1}{1000}$. The phase shift $\exp\left(i\dfrac{\pi\mu_j}{4}\right)$ for each branch is given in Example 5.

Examples 1-4 are 1d examples proposed in [18], and Example 5 is a 2d example proposed in [25], which has a zigzag caustic in both x-direction and y-direction.

Example 1. Constant potential $V(x) = 10$. The initial conditions for the Schrödinger equation are given by:

$$A_0(x) = \exp(-25x^2), \qquad S_0(x) = -\frac{1}{5}\log(2\cosh(5x)).$$

So the initial conditions for the corresponding Liouville equation will be:

$$\rho_0(x) = |A_0(x)|^2 = \exp(-50x^2), \qquad u_0(x) = \partial_x S_0(x) = -\tanh(5x).$$

Figure 1 shows three branches of velocities and phases where the star points are the caustic points.

When $\epsilon = 0.001$, we compare the amplitude of the Schrödinger solution $|\Psi|$ with $|\Phi_1|$ in Figure 2(a), in which one can observe that the only errors are basically the two peaks near the caustic points. We also make comparisons between $|\Psi|$ and $|\Phi_2|$, $|\Phi_3|$ in Figures 2(b)-2(c), in which the errors, besides around the caustic points, are significant elsewhere. The l^1 error plot when ϵ goes to zero is shown in Figure 3. Furthermore, to illustrate the importance of the phase shift, we also compare the position density flux $\frac{\epsilon}{2i}(\Phi_j \nabla\overline{\Phi}_j - \overline{\Phi}_j \nabla\Phi_j)$ and the kinetic energy $\frac{\epsilon^2}{2}|\nabla\Phi_j|^2$ and their Schrödinger counterparts in Figure 4 and Figure 5, $j = 1, 2$. Finally, to show the necessity of using a higher order scheme in the numerical computation of the phase, we give a numerical example in Figure 6 in which the phase is solved spatially by the first order upwind scheme. And it clearly demonstrates that if ϵ is not resolved, one can not get the correct oscillation structure. Besides, Figure 7 shows the numerical results got by using the forward Euler method for the time discretization. To get satisfactory results, we use $\Delta t = \frac{1}{6400}$, which is much smaller than the one used in the second order Runger-Kutta method.

Example 2. Harmonic oscillator $V(x) = \frac{x^2}{2}$. The initial conditions are the same as Example 1.

Similar results got at $\epsilon = 0.001$ and $t = 0.5$ can be found in Figure 8 and Figure 9, where the semiclassical limit Φ_1 gives better approximation around the crest points.

Example 3. A free particle model for a Gaussian pulse with zero potential $V(x) = 0$ and one cusp caustic. The initial conditions for the Schrödinger equation are given by:

$$A_0(x) = \exp(-25x^2), \qquad S_0(x) = \frac{1}{\pi}\cos(\pi x).$$

So the initial conditions for the corresponding Liouville equation will be:

$$\rho_0(x) = |A_0(x)|^2 = \exp(-50x^2), \qquad u_0(x) = \partial_x S_0(x) = -\sin(\pi x).$$

In this example, when $\epsilon = 0.001$ and $t = 0.5$, we get a non-oscillatory bullet-shape solution (Figure 12), although there are still three branches of velocities and phases (Figure

10). Actually there are some oscillations before $t = 0.5$, but they disappear quickly (Figure 11).

Example 4. A free particle model for a Gaussian pulse with zero potential $V(x) = 0$ and two cusp caustics. The initial conditions for the Schrödinger equation are given by:

$$A_0(x) = \exp(-25x^2), \qquad S_0(x) = \frac{1}{\pi}(\cos(\pi x) - \frac{1}{3}\cos^3(\pi x)).$$

So the initial conditions for the corresponding Liouville equation will be:

$$\rho_0(x) = |A_0(x)|^2 = \exp(-50x^2), \qquad u_0(x) = \partial_x S_0(x) = -\sin^3(\pi x).$$

In this example the solution has two cusp caustics which yield five branches of phases (Figure 13). Note that, although there are four caustic points, there are only two blow-up points (Figure 14(a)). The errors of Φ_2 and Φ_3 are much larger than that of Φ_1 away from the caustics (Figure 14).

Example 5. A two dimensional example with zigzag caustics in both x-direction and y-direction. Denote x and y as the two spacial components and $u = \partial_x S(x, y)$, $v = \partial_y S(x, y)$ as the two velocity components. The potential is $V(x, y) = 10$, and the initial conditions for the 2d Schrödinger equation are given by

$$A_0(x, y) = \exp(-25(x^2 + y^2)), \quad S_0(x, y) = -\frac{1}{5}(\log(2\cosh(5x)) + \log(2\cosh(5y))).$$

Therefore the initial conditions for the corresponding Liouville equation will be:

$$\rho_0(x, y) = \exp(-50(x^2 + y^2)), \quad u_0(x, y) = -\tanh(5x), \quad v_0(x, y) = -\tanh(5y).$$

The two zigzag multivalued velocities are given in Figure 15. The caustic curves in $x - y$ plane are given in Figure 17, which develop 9 branches. We list all the domains B_i, $i = 1, \cdots, 9$ with the phase shift for each branch as following:

$$\begin{aligned}
B_1 &= \{(x, y)| - 0.5 \le x \le x_1, -0.5 \le y \le y_1\}, \quad \text{with no phase shift,} \\
B_2 &= \{(x, y)|x_2 \le x \le x_1, -0.5 \le y \le y_1\}, \quad \text{with the phase shift } \exp(-\frac{i\pi}{2}), \\
B_3 &= \{(x, y)|x_2 \le x \le 0.5, -0.5 \le y \le y_1\}, \quad \text{with no phase shift,} \\
B_4 &= \{(x, y)| - 0.5 \le x \le x_1, y_2 \le y \le y_1\}, \quad \text{with the phase shift } \exp(-\frac{i\pi}{2}), \\
B_5 &= \{(x, y)|x_2 \le x \le x_1, y_2 \le y \le y_1\}, \quad \text{with the phase shift } \exp(-i\pi), \\
B_6 &= \{(x, y)|x_2 \le x \le 0.5, y_2 \le y \le y_1\}, \quad \text{with the phase shift } \exp(-\frac{i\pi}{2}), \\
B_7 &= \{(x, y)| - 0.5 \le x \le x_1, y_1 \le y \le 0.5\}, \quad \text{with no phase shift,} \\
B_8 &= \{(x, y)|x_2 \le x \le x_1, y_1 \le y \le 0.5\}, \quad \text{with the phase shift } \exp(-\frac{i\pi}{2}), \\
B_9 &= \{(x, y)|x_2 \le x \le 0.5, y_1 \le y \le 0.5\}, \quad \text{with no phase shift.}
\end{aligned}$$

Let $\epsilon = 0.001$. The solution of Schrödinger equation computed by SP2 at $t = 0.5$ and the semiclassical limit Φ_1 is given in Figure 16. In Figure 17, the left figure shows the error between them, from which one can see that the main error lies near the caustic curves.

6 Conclusion

The level set method proposed in [18, 7, 17] for the computation of multivalued physical observables of the semiclassical limit of the linear Schrödinger equation does not include the proper phase shift across caustics. In this article, we augment the level set method by incorporating the phase shift determined by the Keller-Maslov index. In order to achieve this one needs to track the caustic point or surface, which can be done naturally in the level set framework. We used extensive numerical experiments to demonstrate improved numerical accuracy of the new approach away from the caustics.

Acknowledgement

The first author thanks Professor Stanley Osher on the discussion about the presentation of an earlier version of the paper. The second author gives thanks to Professors K. Novak and L. Gosse for their valuable discussions.

References

[1] W. Bao, S. Jin and P. A. Markowich, On Time-Splitting Spectral Approximations for the Schrödinger Equation in the Semiclassical Regime, *J. Comput. Phys.* 175 (2002), no. 2, 487–524.

[2] J. D. Benamou, O. Lafitte, R. Sentis and I. Solliec, A Geometric Optics Based Numerical Method for High Frequency Electromagnetic Fields Computations near Fold Caustics - Part I, *J. Comput. Appl. Math.*, 156 (2003), no. 1, 93–125.

[3] J. D. Benamou, O. Lafitte, R. Sentis and I. Solliec, A Geometric Optics Based Numerical Method for High Frequency Electromagnetic Fields Computations near Fold Caustics - Part II, *J. Comput. Appl. Math.*, 167 (2004), no. 1, 91–134.

[4] C. M. Bender and S. A. Orszag, **Advanced Mathematical Methods for Scientists and Engineers**, McGraw-Hill, New York, 1978.

[5] Y. Brenier and L. Corrias, A kinetic formulation for multibranch entropy solutions of scalar conservation laws, Ann. Inst. Henry Poincaré, 15(2): 169-190, 1998.

[6] R. Carles and L. Gosse, Numerical Aspects of Nonlinear Schrödinger Equations in the Presence of Caustics, *preprint*.

[7] L.-T. Cheng, H. Liu, and S. Osher, Computational High-frequency Wave Propagation Using the Level Set Method, with Applications to the Semi-classical Limit of Schrödinger equations, *Comm. Math. Sci.*, 1(3) (2003), 593-621.

[8] J. J. Duistermaat, Fourier Integral Operators. Birkhäuser, 1995.

[9] B. Engquist, E. Fatemi, S. Osher, Numerical Solution of the High Frequency Asymptotic Expansion for the Scalar Wave Equation, *J. Comput. Phys.*, 120 (1) (1995), 145-155.

[10] B. Engquist and O. Runborg, Multi-phase Computations in Geometrical Optics, *J. Comput. Appl. Math.*, 74 (1996), 175-192.

[11] L. C. Evans, **Partial Differential Equations**, American Mathematical Society, USA, 1998.

[12] I. Gasser, P.A. Markowich, Quantum Hydrodynamics, Wigner transforms and the classical limits, Asymptotic Analysis 14 (1997) 97-116.

[13] P. Gerard, P. A. Markowich, N. J. Mauser and F. Poupaud, Homogenization Limits and Wigner Transforms, *Comm. Pure Appl. Math.*, 50 (4) (1997), 323-379.

[14] L. Gosse, Using K-Branch Entropy Solutions for Multivalued Geometric Optics Computations, *J. Comput. Phys.* 180 (2002), no. 1, 155–182.

[15] L. Gosse, S. Jin and X. T. Li, On Two Moment Systems for Computing Multiphase semiclassical Limits of the Schrödinger Equation, *Math. Models Meth. Appl. Sci.* 13 (2003), No. 12, 1689-1723.

[16] S. Jin and X. T. Li, Multi-phase Computations of the Semiclassical Limit of the Schrödinger Equation and Related Problems: Whitham vs. Wigner, *Physica D* 182 (2003), 46-85.

[17] S. Jin, H. Liu, S. Osher and R. Tsai, Computing multi-valued physical observables the semiclassical limit of the Schrödinger equations, *J. Comp. Phys.*, 205, (2005), 222-241.

[18] S. Jin and S. Osher, A Level Set Method for the Computation of Multivalued Solutions to Quasi-Linear Hyperbolic PDEs and Hamilton-Jacobi Equations, *Comm. Math. Sci.*, 1(3) (2003), 575-591.

[19] P. L. Lions, T. Paul, Sur les Measures de Wigner, *Revista. Mat. Iberoamericana* 9 (1993), 553-618.

[20] P. L. Lions, P. E. Souganidis, Convergence of MUSCL and Filtered Schemes for Scalar Conservation Laws and Hamilton-Jacobi Equations, *Numer. Math.* 69 (4) (1995), 441-470.

[21] P. A. Markowich, P. Pietra and C. Pohl, Numerical Approximation of Quadratic obaservables of Schrödinger-type equations in the semiclassical limit, *Numer. Math.*, 81 (1999), 595-630.

[22] P. A. Markowich, P. Pietra, C. Pohl and H. P. Stimming, A Wigner-Measure Analysis of the Dufort-Frankel Scheme for the Schrödinger equation, *SIAM J. Num. Anal.*, 40 (2002), 1281-1310.

[23] V.P. Maslov, **Semiclassical Approximation in Quantum Mechanics**, Reidel Dordrecht, 1981.

[24] C. Min, Simplicial Isosurfacing in Arbitrary Dimension and Codimension, *J. Comp. Phys.*, 190 (2003), no.1, 295–310.

[25] S. Osher, L.-T. Cheng, M. Kang, H. Shim and Y.-H. Tsai, Geometric Optics in a Phase-space-based Level Set and Eulerian Framework, *J. Comput. Phys.*, 179 (2002), 622-648.

[26] D. Peng, B. Merriman, S. Osher, H. Zhao and M. Kang, A PDE Based Fast Local Level Set Method, *J. Comput. Phys.*, 155 (1999), 410-438.

[27] J. Qian, L.-T. Cheng, and S. Osher, A Level Set Based Eulerian Approach for Anisotropic Wave Propagation, *Wave Motion*, 37 (2003), 365-379.

[28] G. B. Whitham, **Linear and Nonlinear Waves**, Wiley, New York, 1974.

[29] E. Wigner, On the Quantum Correction for Thermodynamic Equilibrium, *Phys. Rev.*, 40 (1932), 749-759.

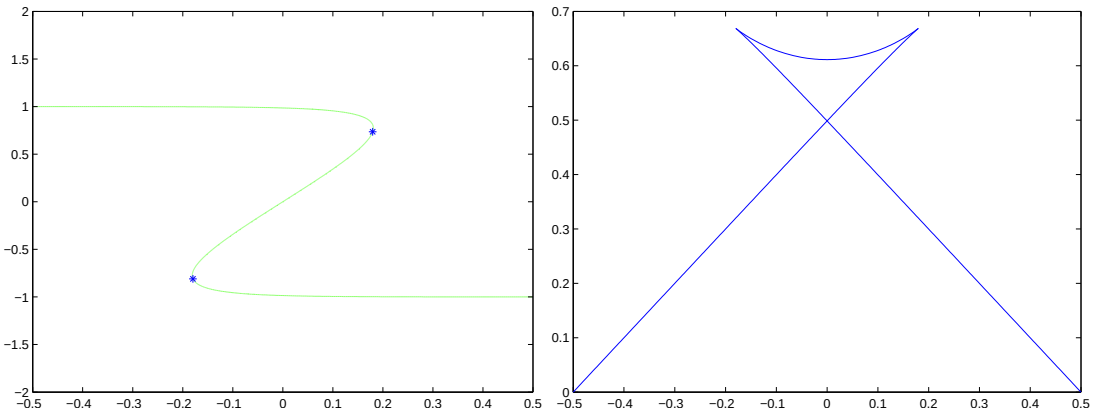

Figure 1: Example 1, the left figure is the multivalued velocity in the phase plane, where '*' represents the caustic points; the right figure shows the multivalued phase.

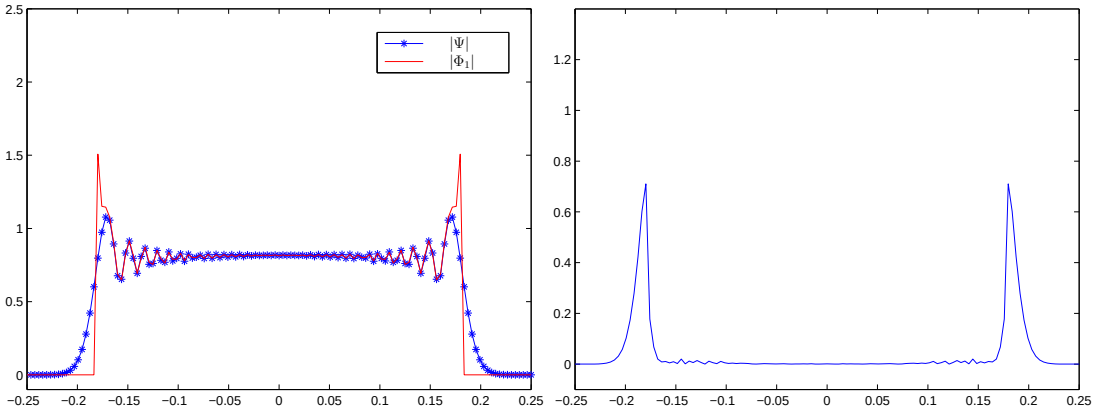

(a) The wave amplitude of Schrödinger solution $|\Psi|$ versus $|\Phi_1|$

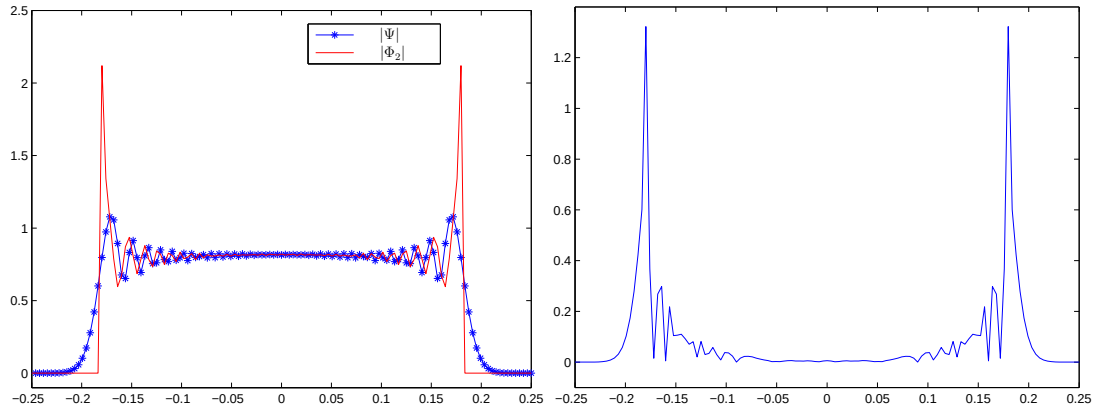

(b) The wave amplitude of Schrödinger solution $|\Psi|$ and versus $|\Phi_2|$

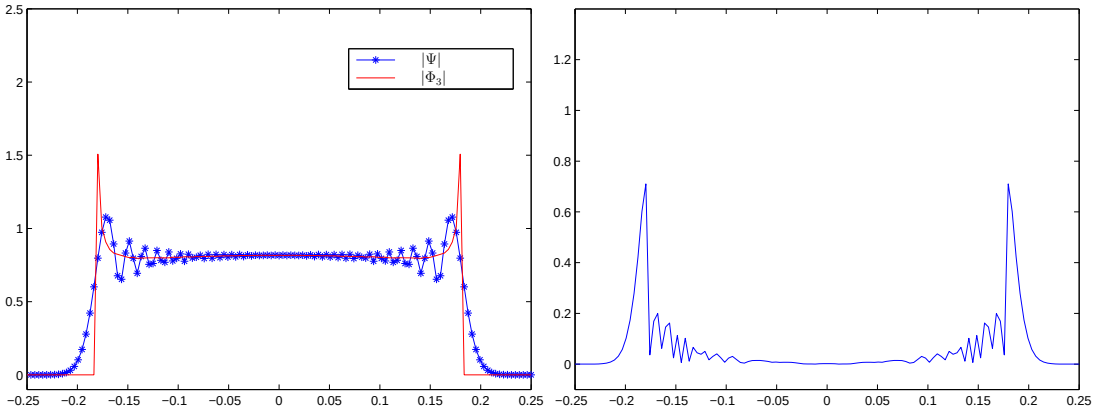

(c) The wave amplitude of Schrödinger solution $|\Psi|$ versus $|\Phi_3|$

Figure 2: Example 1, at $\epsilon = 0.001$ and $t = 0.5$, the left figures are the comparisons of the wave amplitude between the Schrödinger solution Ψ and the three numerical results Φ_1, Φ_2 and Φ_3; the right figures show the difference between them: $||\Psi| - |\Phi_j||, j = 1, 2, 3$.

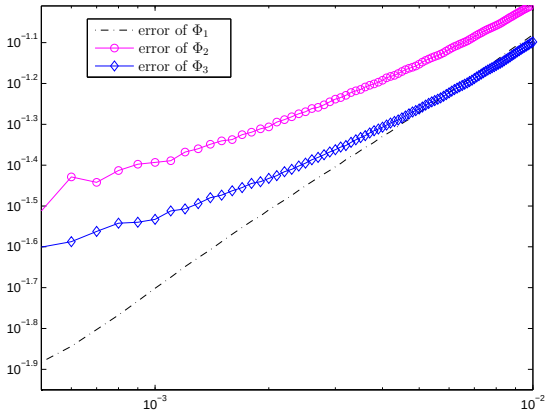

Figure 3: Example 1, the log-log figure of the error $\int_{-0.5}^{0.5} ||\Psi| - |\Phi_j||\, dx$ as ϵ goes to 0 where Ψ is the Schrödinger solution and Φ_j, $j = 1, 2, 3$ are defined in (5.1)-(5.3).

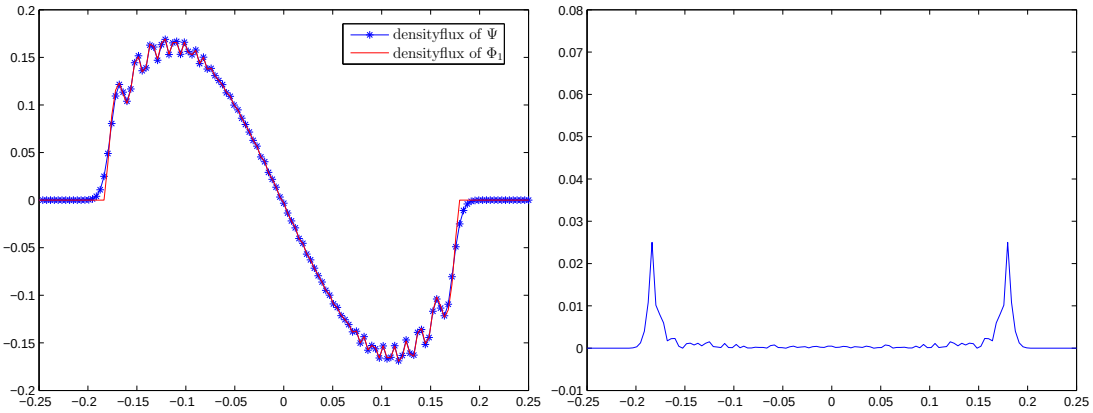

(a) The density flux of Schrödinger solution Ψ and the semiclassical limit Φ_1

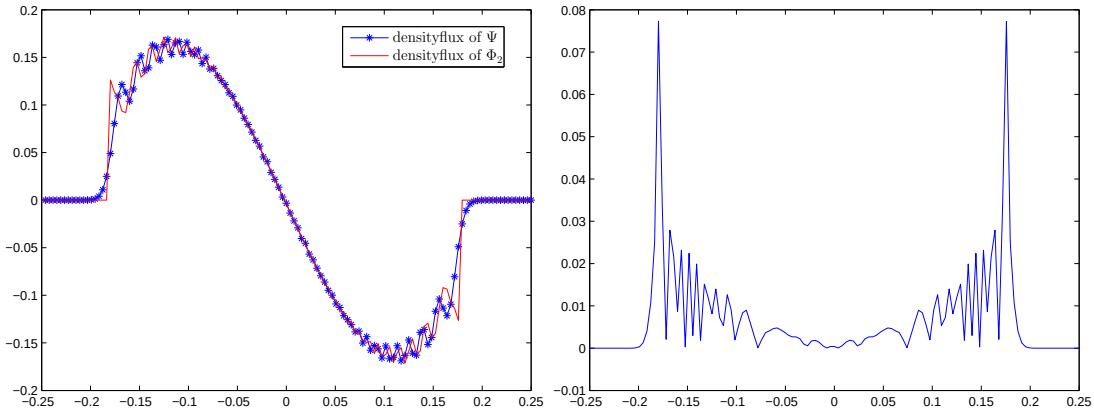

(b) The density flux of Schrödinger solution Ψ and the semiclassical limit Φ_2

Figure 4: Example 1, at $\epsilon = 0.001$ and $t = 0.5$, the left figures are the comparisons of the position density flux between the Schrödinger solution Ψ and the numerical solutions Φ_1 and Φ_2; the right figures show the error between the Schrödinger solution and the corresponding numerical counterparts.

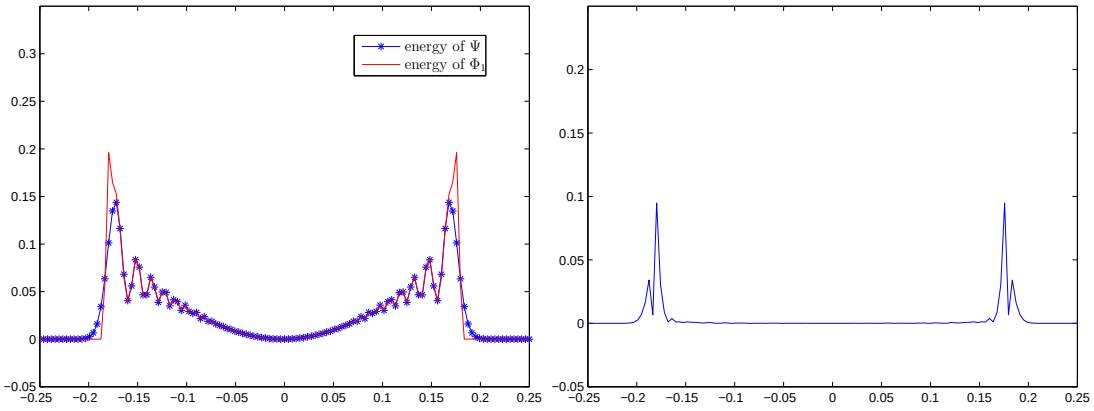

(a) The kinetic energy of Schrödinger solution Ψ and the semiclassical limit Φ_1

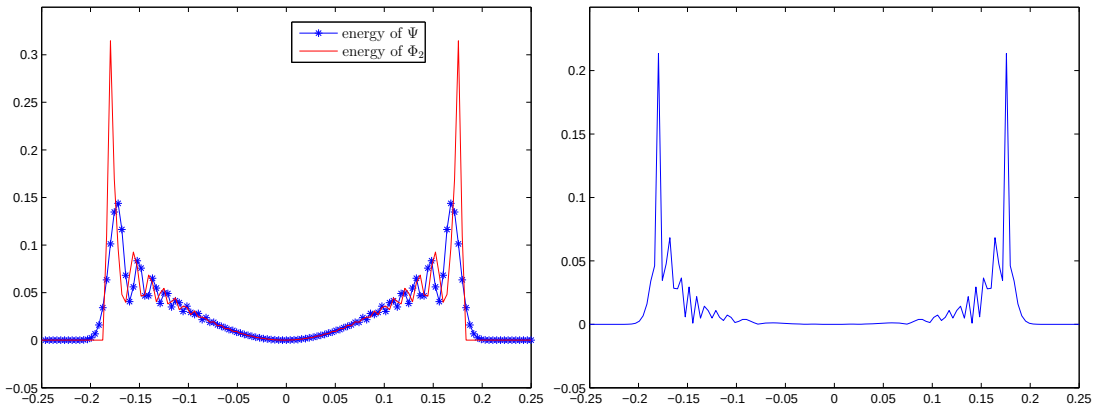

(b) The kinetic energy of Schrödinger solution Ψ and the semiclassical limit Φ_2

Figure 5: Example 1, at $\epsilon = 0.001$ and $t = 0.5$, the left figures illustrate the comparison of the kinetic energy between the Schrödinger solution and the numerical solutions Φ_1 and Φ_2; the right figures show the difference between them.

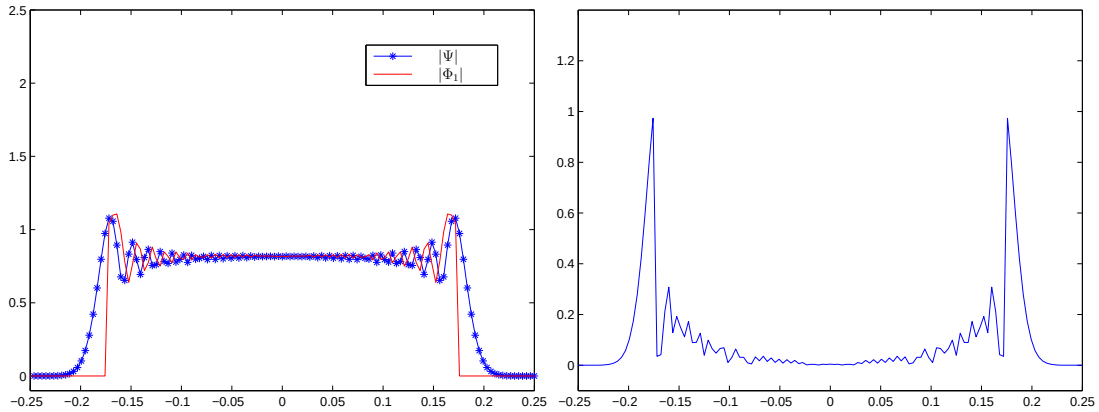

Figure 6: Example 1, at $\epsilon = 0.001$ and $t = 0.5$, the left figure illustrates the comparison of the wave amplitude between the Schrödinger solution Ψ and the semiclassical limit Φ_1, where the phase is solved by the first order upwind scheme; the right figure shows the difference between them.

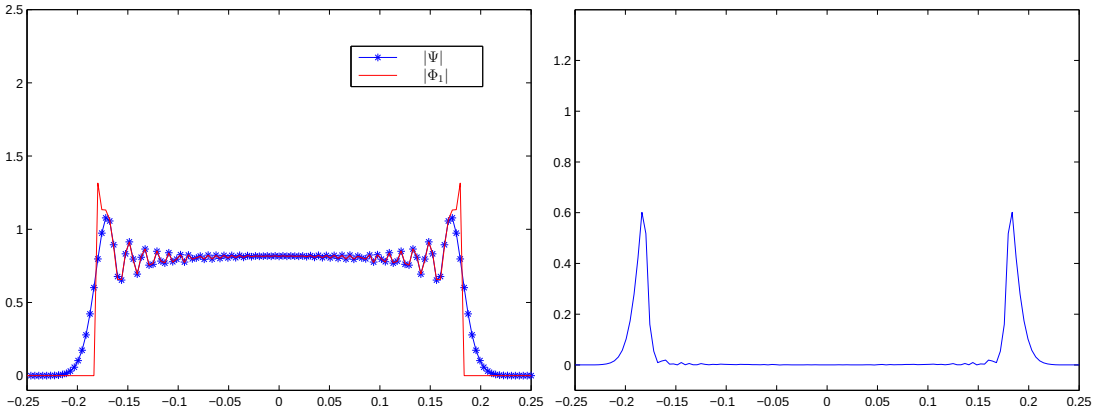

Figure 7: Example 1, at $\epsilon = 0.001$ and $t = 0.5$, the left figures illustrate the comparison of the wave amplitude between the Schrödinger solution Ψ and the semiclassical limit Φ_1, where the phase is solved by the second order upwind scheme in space and the forward Euler scheme in time; the right figures show the difference between them.

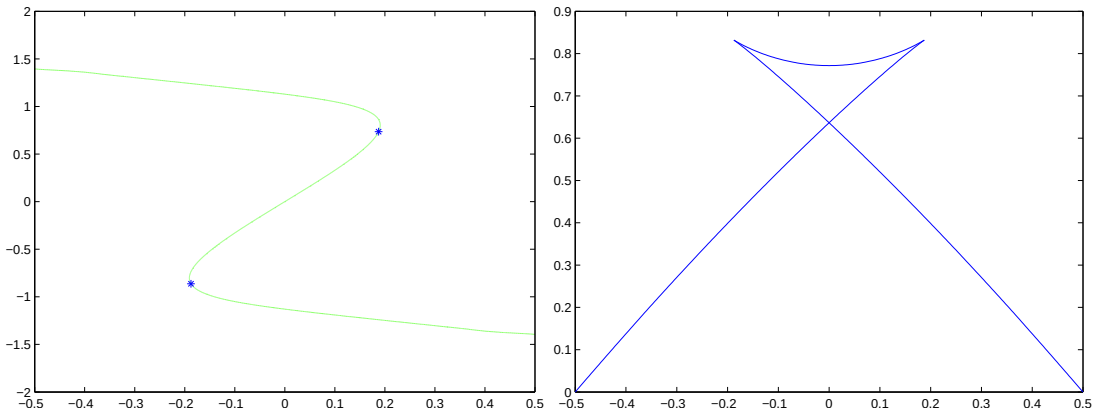

Figure 8: Example 2, the left figure is the multivalued velocity in the phase plane, where '*' represents the caustic points; the right figure shows the multivalued phase.

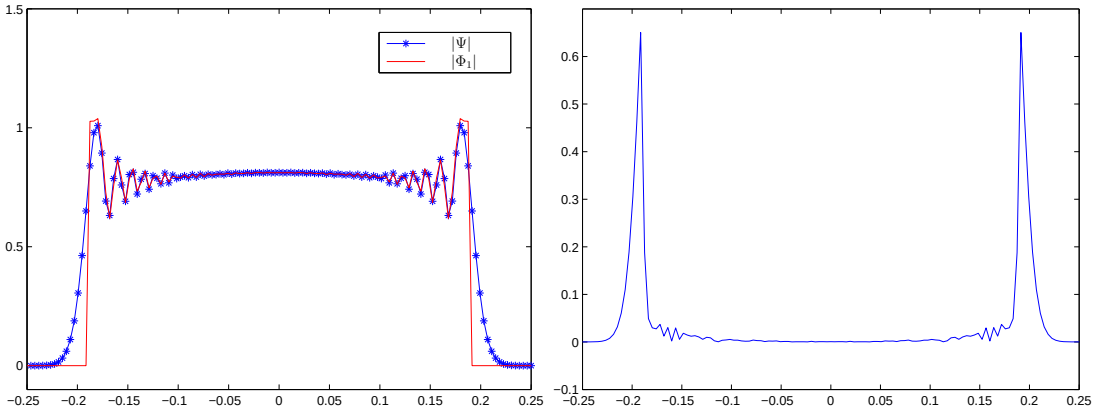

(a) The wave amplitude of Schrödinger solution $|\Psi|$ and the semiclassical limit $|\Phi_1|$

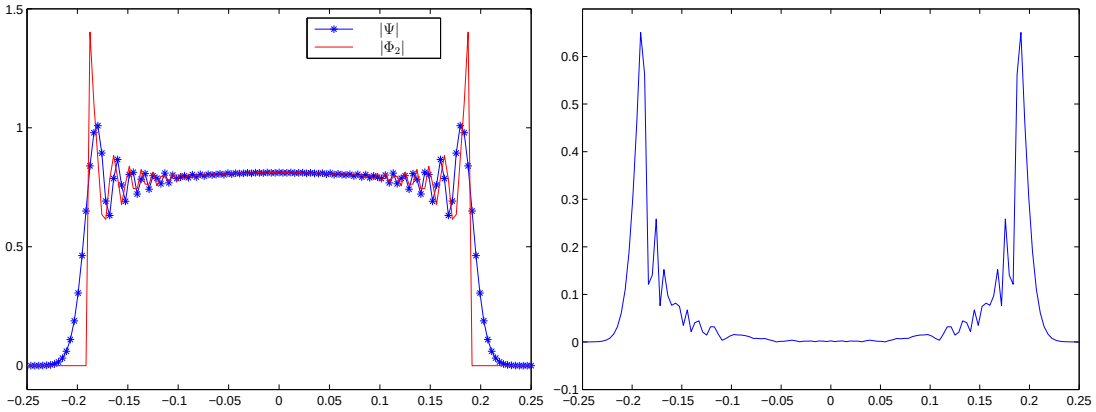

(b) The wave amplitude of Schrödinger solution $|\Psi|$ and the semiclassical limit $|\Phi_2|$

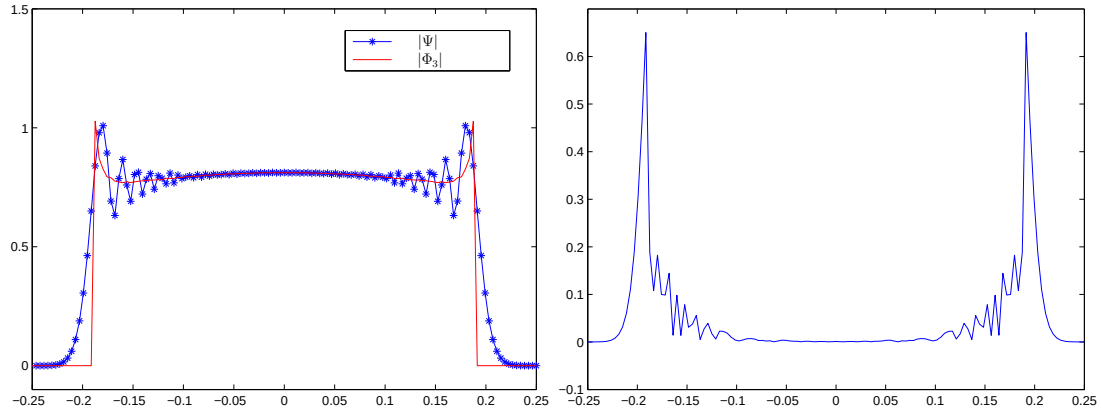

(c) The wave amplitude of Schrödinger solution $|\Psi|$ and the total density $|\Phi_3|$

Figure 9: Example 2, at $\epsilon = 0.001$ and $t = 0.5$, the left figure illustrates the comparison of the wave amplitude between the Schrödinger solution Ψ and the three numerical results Φ_1, Φ_2 and Φ_3; the right figure shows the difference between them: $||\Psi| - |\Phi_j||, j = 1, 2, 3$.

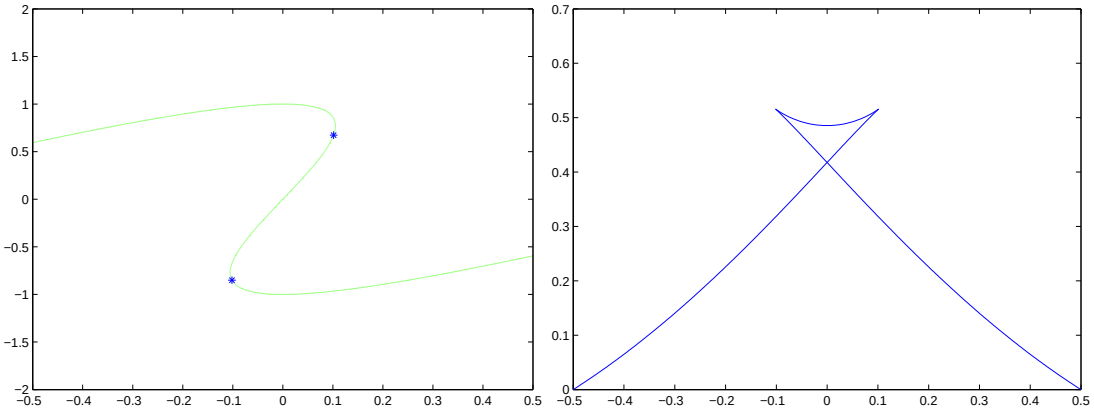

Figure 10: Example 3, the left figure is the multivalued velocity in the phase plane, where '*' represents the caustic points; the right figure shows the multivalued phase.

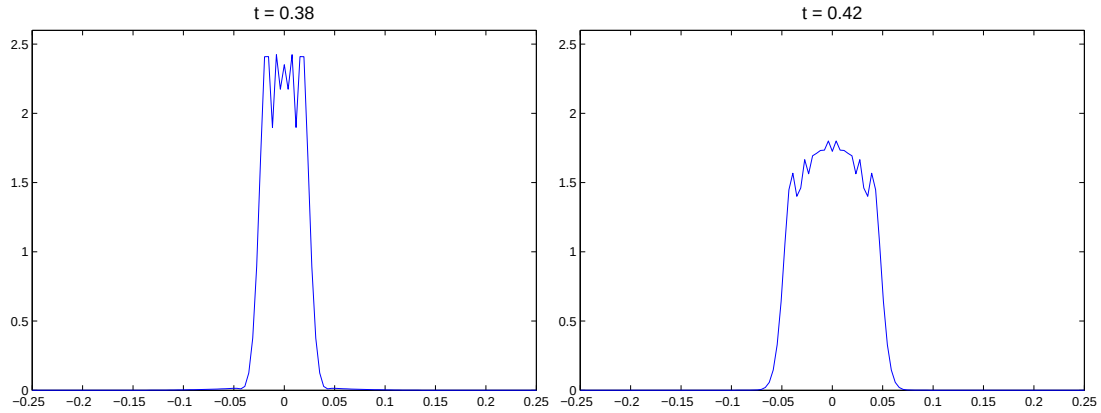

Figure 11: Example 3, the schrödinger solution. Left: at $t = 0.38$; right: at $t = 0.42$. The mesh size is $\Delta x = \dfrac{1}{16384}$ in the SP2 method.

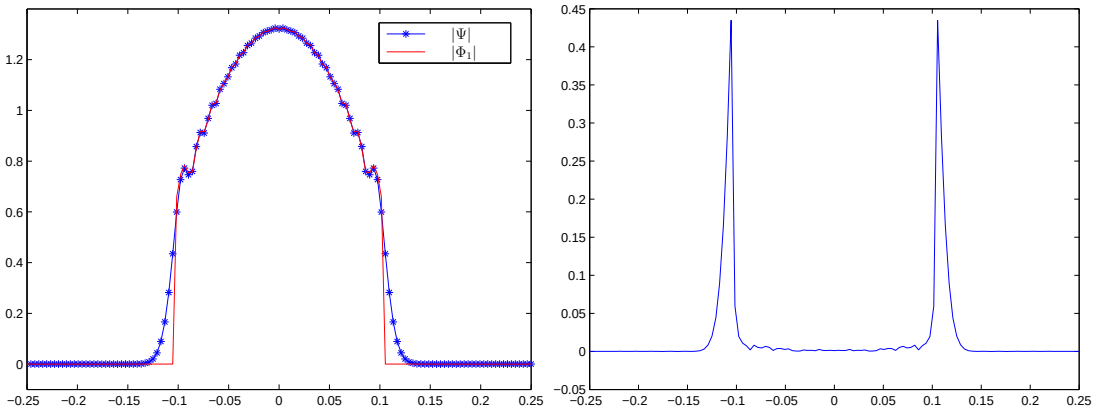

(a) The wave amplitude of Schrödinger solution $|\Psi|$ and the semiclassical limit $|\Phi_1|$

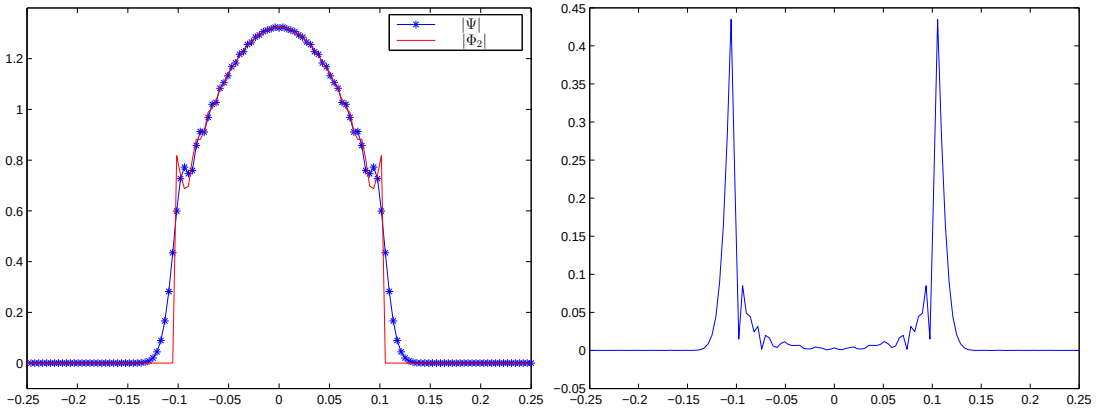

(b) The wave amplitude of Schrödinger solution $|\Psi|$ and the semiclassical limit $|\Phi_2|$

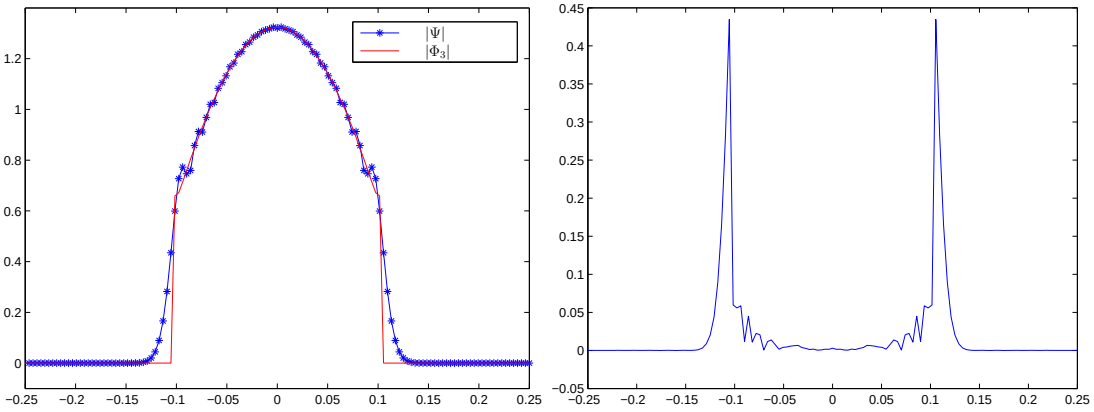

(c) The wave amplitude of Schrödinger solution $|\Psi|$ and the total density $|\Phi_3|$

Figure 12: Example 3, at $\epsilon = 0.001$ and $t = 0.5$, the left figure illustrates the comparison of the wave amplitude between the Schrödinger solution Ψ and the three numerical results Φ_1, Φ_2 and Φ_3; the right figure shows the difference between them: $||\Psi| - |\Phi_j||, j = 1, 2, 3$.

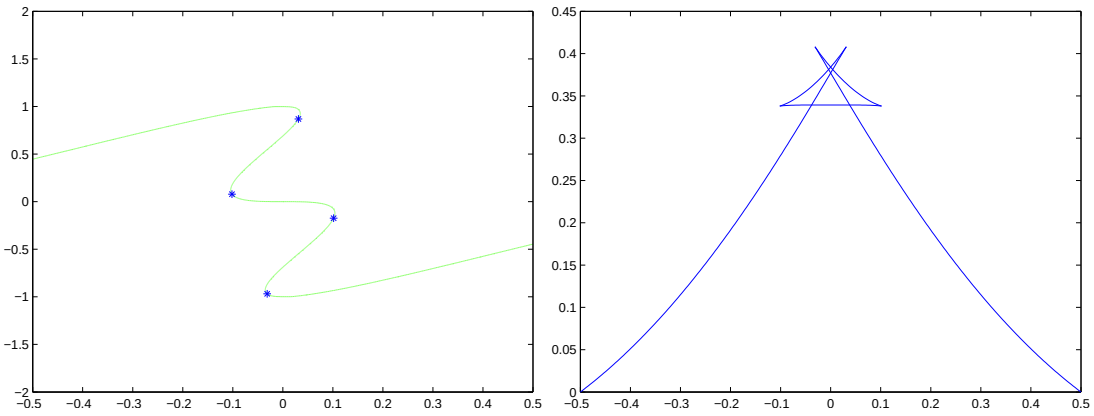

Figure 13: Example 4, the left figure is the multivalued velocity in the phase plane, where '*' represents the caustic points; the right figure shows the multivalued phase.

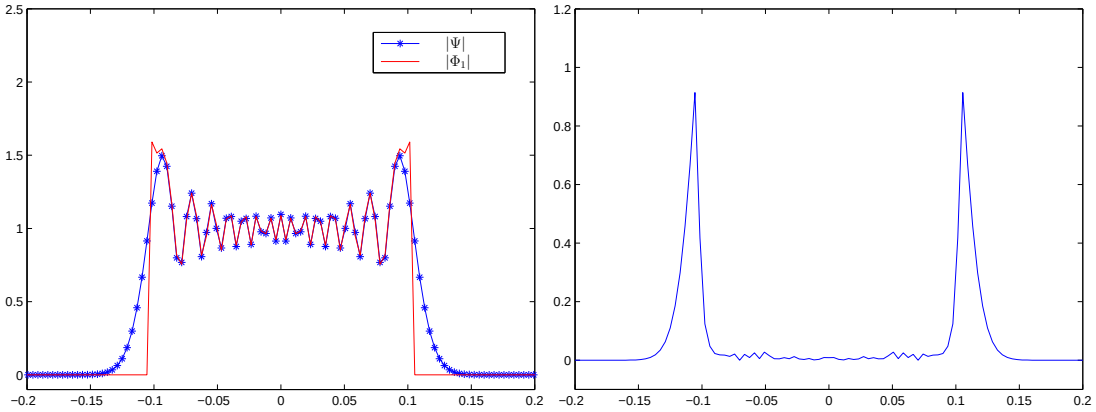

(a) The wave amplitude of Schrödinger solution $|\Psi|$ and the semiclassical limit $|\Phi_1|$

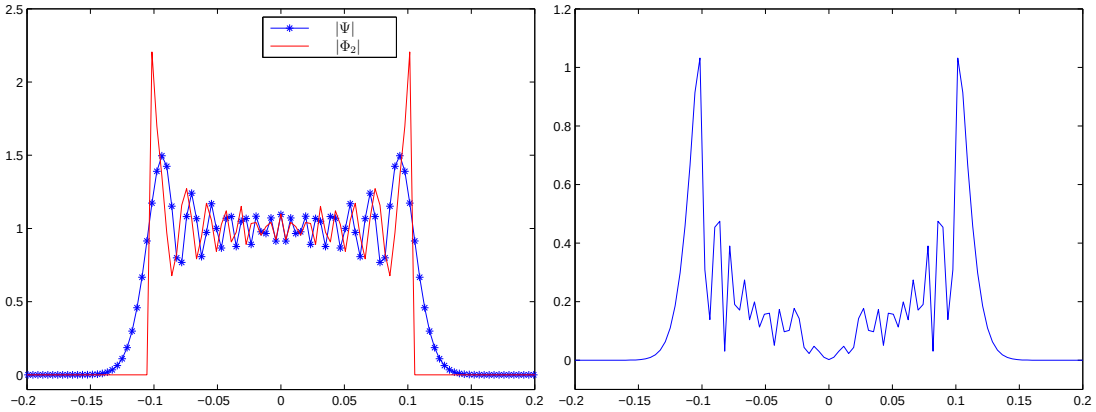

(b) The wave amplitude of Schrödinger solution $|\Psi|$ and the semiclassical limit $|\Phi_2|$

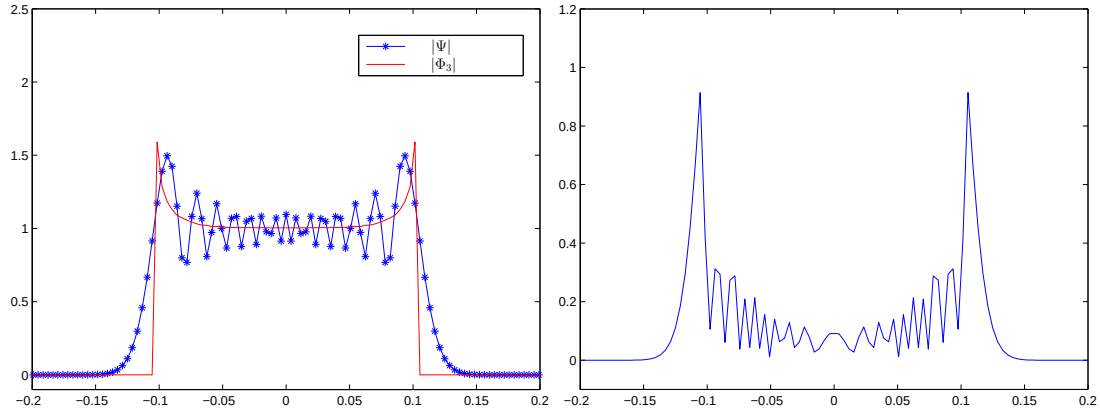

(c) The wave amplitude of Schrödinger solution $|\Psi|$ and the total density $|\Phi_3|$

Figure 14: Example 4, at $\epsilon = 0.001$ and $t = 0.5$, the left figure illustrates the comparison of the wave amplitude between the Schrödinger solution Ψ and the three numerical results Φ_1, Φ_2 and Φ_3; the right figure shows the difference between them: $||\Psi| - |\Phi_j||, j = 1, 2, 3$.

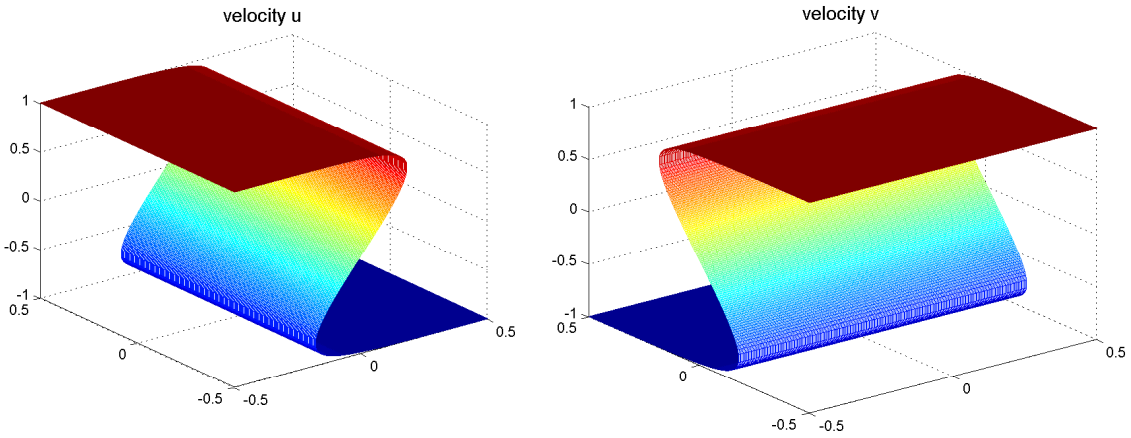

Figure 15: Example 5, at $\epsilon = 0.001$ and $t = 0.5$, the left figure shows the x-direction velocity u; the right figure shows the y-direction velocity v. $\Delta x = \Delta y = \Delta u = \Delta v = \dfrac{1}{256}$.

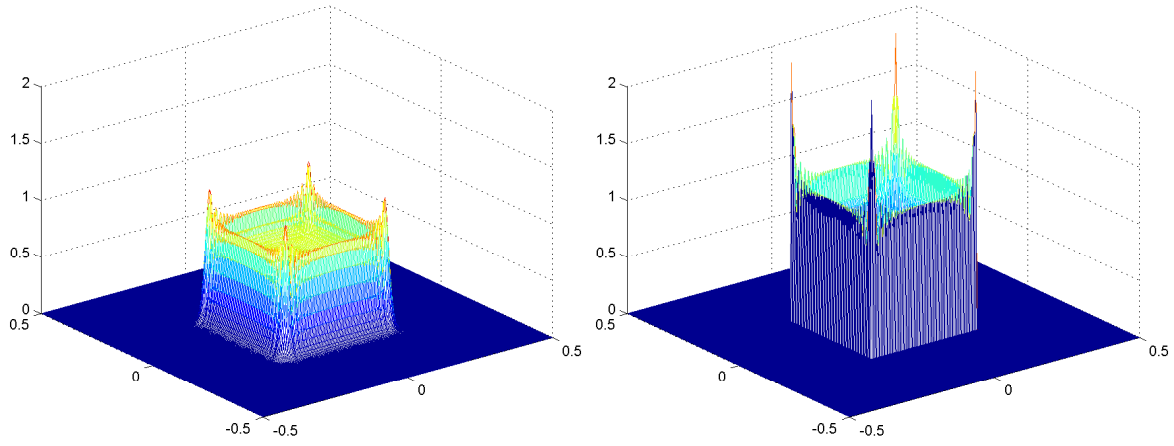

Figure 16: Example 5, at $\epsilon = 0.001$ and $t = 0.5$, the left figure shows the amplitude of the schrödinger solution $|\Psi|$; the right one shows the amplitude of the semiclassical solution $|\Phi_1|$.

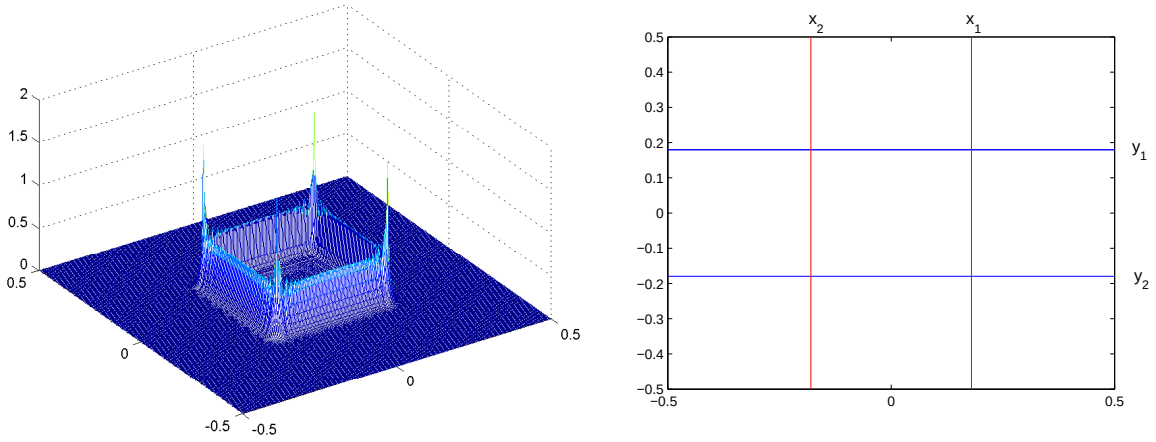

Figure 17: Example 5, at $\epsilon = 0.001$ and $t = 0.5$, the left figure shows the error between the Schrödinger solution $|\Psi|$ and $|\Phi_1|$; the right figure shows the caustic curves in the $x - y$ plane, in which $x_1 = y_1 = 0.1797$, $x_2 = y_2 = -0.1797$.